Determination of the Aggregate Binding Site of Amyloid Protofi-brils Using Electron Capture Dissociation Tandem MS

Yuko P. Y. Lam[1], Christopher A. Wootton[1], Ian Hands-Portman[2], Juan Wei[1], Cookson K. C. Chiu[1], I. Romero-Canelon[1,3], Frederik Lermyte[1], Mark P. Barrow[1], Peter B. O'Connor[1]

[1]Department of Chemistry, Gibbet Hill Road, University of Warwick, Coventry CV4 7AL, United Kingdom

[2]Department of Life Sciences, Gibbet Hill Campus, University of Warwick, Coventry CV4 7AL, United Kingdom

[3]School of Pharmacy, University of Birmingham, Edgbaston, Birmingham B15 2TT, United Kingdom

ABSTRACT: Amyloid fibril formation is a hallmark in a range of human diseases. Analysis of the molecular details of amyloid aggregation, however, are limited by the difficulties in solubilising, separating, and identifying the aggregated biomolecules. Additional labelling or protein modification are required in many current analytical techniques in order to provide molecular details of amyloid protein aggregation, but these modifications may result in protein structure disruption. Herein, ultrahigh resolution mass spectrometry (MS) with electron capture dissociation tandem MS (ECD MS/MS) has been applied to monitor the formation of early oligomers of human islet amyloid polypeptide (hIAPP) which aggregates rapidly in the pancreas of type II diabetes (T2D) patients. ECD MS/MS results show the aggregation region of the early oligomers is at Ser-28/Ser-29 residue of a hIAPP unit and at Asn-35 residue

of another hIAPP unit near the C-terminus in gas phase. These data contribute to the understanding of binding site between hIAPP units which may help for the specific target region therapeutic development in the future. Furthermore, MS has also applied to quantify the amount of soluble amyloid protein remaining in the incubated solutions, which can be used to estimate the aggregation rate of amyloid protein during incubation (28 days). These data are further correlated with the results obtained using fluorescence spectroscopy and transmission electron micros-copy (TEM) to generate a general overview of amyloid protein aggregation. The methods demonstrated in this article not only explore the aggregation site of hIAPP down to an amino acid residue level, but are also applicable to many amyloid protein aggregation studies.

Introduction

Amyloid fibril formation is a hallmark in a range of human diseases, including Alzheimer's disease,[1] Parkinson's disease,[2] and type II diabetes (T2D).[3] An amyloid fibril is composed of insoluble aggregates originating from smaller, soluble monomer peptides, which are believed to refold into crossed β-strands perpendicular to the fibril axis.[4-5] The overall structures of amyloid fibrils have been studied in detail for more than a half-century;[6-8] the molecular details of aggregation, however, are still limited by the difficulties in solubilising, separating, and identifying the aggregated biomolecules.

Human islet amyloid polypeptide (hIAPP; also referred to as amylin) is a 37-residue hormone peptide (Figure 1A) co-secreted with insulin and involved in regulating blood glucose levels.[9-10] The concentration of hIAPP is around 1% - 2%

relative to the level of insulin in secretory granules.[11] hIAPP contains an intramolecular disulfide bond between Cys-2 and Cys-7 as well as an amidated C-terminus,[12] and is an intrinsically disordered protein with a low level of persistent helical structure between residues Asn-3 and Leu-27 in solution.[13] Early oligomers of hIAPP have been shown to be a key factor in causing the decline of pancreatic β-cell mass and the failure of islet cell transplants used for the treatment of T2D.[14-15] In the past decade, electron microscopy, circular dichroism (CD), and computational modelling simulations have been the common techniques for studying hIAPP aggregates, and a solid β-sheet structure was observed in the mature hIAPP fibrils.[16-19] However, the aggregation mechanism remains poorly understood.[20]

Computational docking simulations with residue replacement techniques have been applied to estimate the aggregation mechanism of hIAPP based on its molecular structure.[17] Computational models suggested Phe-15, in the α-helix region of hIAPP, was a critical residue for the aggregation since the *in silico* rate of fibril formation was significantly reduced in the mutants where the Phe-15 residue was replaced (F15D and F15K mutant hIAPP). Nuclear magnetic resonance (NMR) spectroscopy experiments led to the interpretation that the N-terminal segment of hIAPP (residues 1 – 17) was essential for the formation of amyloid fibrils.[21] These models contrast with other hypotheses that the region of hIAPP between residues 20-29 contains amyloidogenic tendency, which was demonstrated by comparing the rate of fibril formation between the rat IAPP (rIAPP) and hIAPP.[16] Rat and human IAPP sequences differ by six amino acid residues (of the 37 present), five of which are located within residues 20-29; however, experimental data has shown rIAPP did not aggregate over a 5-day incubation period while hIAPP was shown to aggregate

readily within 20 hours.[16, 22] This hypothesis has been further explored on multiple occasions using short sections of hIAPP to identify the active aggregation region. Several studies using peptides containing residues 20-29 were shown to aggregate effectively,[22-30] indicating the active aggregation region could be within this range. Following this, solid state NMR also revealed that hIAPP units stack to form β-strands and then further aggregate into layers of parallel β-sheets.[12] Ion mobility mass spectrometry (IM-MS) was recently used for the study of hIAPP aggregation.[4, 31-35] The structures of monomer and oligomers were predicted by molecular dynamics modelling based on the collision cross section area obtained from IM-MS [34, 36-37]. β-strand interaction was determined as the most stable and favourable binding motif in the hIAPP dimer.[33] A fragment of hIAPP (residue 24 – 27) has been shown to be non-amyloidogenic;[25] while another fragment of hIAPP (residues 28-33) was proposed by Bleiholder *et al.* as an amyloidogenic region via a 'steric zipper' assembly pathway using IM-MS.[4] Early oligomers of hIAPP are toxic to the β-cells;[38] however, the conflicting reports on the binding motif hinder drug development. Improved understanding of the binding motif of hIAPP is therefore required.

Non-covalent interactions between proteins and protein-ligands are commonly observed; however, it is challenging to localise the interaction sites between these molecules as the non-covalent bonds are weaker than the covalent bonds in protein backbone, which results in fragmentation at the non-covalent interaction site when using collisionally activated dissociation (CAD) and infrared multiphoton dissociation tandem MS (IRMPD MS/MS), losing structural information. However, electron capture dissociation (ECD) MS/MS can localise the interaction site of proteins and

protein-ligand complexes by fragmenting the protein backbone while preserving the non-covalent bonding.[39-41] Using ECD MS/MS, the non-covalent interaction sites between proteins and protein-ligands can be located quite accurately, often to several amino acid residues.

Herein, Fourier transform ion cyclotron resonance mass spectrometry (FTICR MS) is applied in monitoring the aggregation of hIAPP. ECD MS/MS is used for determining the aggregation sites between the monomer subunits within the dimer and the trimer of hIAPP and localising the binding area to the amino acid residue level without disrupting remaining non-covalent bonds. A synthetic 8-residue segment from hIAPP is used to evaluate the critical aggregation region proposed from the ECD MS/MS results. The concentration of soluble hIAPP is recorded periodically for 28 days in order to study the rate of aggregation in a long-term incubation period. Thioflavin T (ThT) fluorescence spectroscopy and transmission electron microscopy (TEM) are also employed to monitor the rate of fibril formation. The experimental results reveal the aggregation motif of hIAPP as well as the aggregation rate of hIAPP in aqueous solution.

Experimental Section

Sample preparation for early oligomers in hIAPP, the synthetic ^{30}TNVGSNTY^{37}-NH$_2$ peptide, and the mixture of hIAPP & ^{30}TNVGSNTY^{37}-NH$_2$. hIAPP lyophilised powder (Sigma Aldrich Company Ltd, Dorset, England; Figure S1 – S2) and the synthetic ^{30}TNVGSNTY^{37}-NH$_2$ peptide (Eurogentec, England) were initially dissolved in 100% dimethyl sulfoxide (DMSO) at a concentration of 500 μM for storage (at -80ºC) in order to minimise the aggregation rate, as used by Abedini *et*

al..[42] The 500 μM stock solutions were further diluted with high purity Milli-Q (Direct-Q® 3 UV System, Millipore Corporation, US) H_2O (~pH 7.5) to 10 μM solutions, and the final concentrations of DMSO in each solution was 2% (v/v)hIAPP lyophilised powder was also dissolved in Milli-Q H_2O at a concentration of 500 μM and further diluted into 10 uM solution. The mixture of hIAPP & ^{30}TNVGSNTY^{37}-NH_2 was prepared by mixing 10 μM hIAPP (in H_2O) with 10 μM ^{30}TNVGSNTY^{37}-NH_2 (in 100% DMSO) in 1:1 ratio in aqueous solution, and the final concentration of DMSO in hIAPP aqueous solutions was 1% (v/v).

Sample preparation for incubated hIAPP. The 10 μM hIAPP aqueous solution (2000 μL) was incubated for 28 days; 50 μL solution was collected each day. Each collected aliquot solution was then centrifuged at 14,000 rpm for one hour to separate the soluble hIAPP (supernatant) from the insoluble hIAPP fibril. The supernatant solution containing soluble hIAPP was diluted 20-fold with 49.5:49.5:1 water/acetonitrile/formic acid prior to MS analysis.

FTICR MS analysis. Mass spectra were acquired on a 12 tesla solariX FTICR MS (Bruker Daltonik GmbH, Bremen, Germany). All samples were analysed in positive ionisation mode. For the early oligomers study, nano-electrospray ionisation (nESI) with a capillary voltage of 0.6 – 1 kV was applied and the source temperature was set to 80ºC. The nESI glass capillaries were purchased from World Precision Instruments and pulled on a Sutter P-97 capillary puller instrument (One Digital Drive Novato, California, USA). For the detection of deamidated hIAPP and dissociated fibrils, an Apollo II electrospray ionisation (ESI) source (Bruker Daltonik GmbH, Bremen, Germany) was used with a capillary voltage of 4-4.5 kV. The ESI

flow rate was optimised to 100-150 μL/h and the source temperature was set to 200°C. Ions were externally accumulated in a hexapole collision cell before transferred to an infinity cell (ICR cell) for excitation and detection.[43] Data obtained from FTICR-MS were analysed using Bruker DataAnalysis 4.2 software (Bruker Daltonics, Bremen, Germany).

MS/MS fragmentation in the FTICR MS. For the CAD experiments, precursor ions were first isolated using the quadrupole mass filter, then collided with argon gas and accumulated in the collision cell. The collision energy was optimised to 2-18 V and the ion accumulation time to 1-3 seconds. Fragments were then transferred to the infinity cell for detection. For the ECD experiments, precursor ions were first isolated using the quadrupole with a wide mass-to-charge isolation window (~100 Da) and accumulated in the collision cell for 1-3 seconds. Ions were then transferred to the infinity cell, further isolated using Multi-CHEF isolation[44] with an excitation power of 45-55%, and then irradiated with 1.2 eV electrons from a 1.5 A heated hollow cathode. For the infrared-ECD (IR-ECD) experiments, a 25 W continuous-wave CO_2 infrared laser (Synrad Inc, US) was used to activate the protein during ECD in order to increase the fragmentation efficiency.[45] The pulse length and laser power were optimised to 20-50 ms and 12.5 W (50% power) respectively, which is just below the influence threshold for obtaining IRMPD fragment ions. The most intense isotopic peak from each fragment with signal-to-noise ratio (S/N) over 5 was manually assigned. All fragmentation spectra were internally calibrated and species assigned with an uncertainty less than 1 part-per-million (ppm) (Table S1 – S10).

Studying intermolecular binding strength within oligomers via FTICR

MS/MS. The area of the highest isotopic peak of each oligomer was measured using Bruker DataAnalysis 4.2 software. The percentage of dimer ion (%) was calculated as follows:

$$\text{Dimer (\%)} = \frac{\text{Peak area of dimer}}{\text{Peak area of monomer+ dimer}} \times 100\%$$

A dissociation curve for dimer ions was obtained by plotting the percentage of dimer remaining against the CAD energy used. The same calculation method was applied to obtain the dissociation curve of other oligomer ions.

Transmission electron microscopy (TEM). The TEM images of the incubated solutions, including 10 μM hIAPP solutions, 10 μM synthetic ^{30}TNVGSNTY^{37}-NH_2 solution, and the mixture of hIAPP & ^{30}TNVGSNTY^{37}-NH_2 solution, were acquired on a Jeol 2010F TEM (JEOL UK Ltd. Hertfordshire, UK) operated at 200 kV. 10 μL of incubated solution was transferred onto a carbon-coated grid and settled for one minute, followed by removing the excess solution using filter paper. A 2% (w/v) uranyl acetate solution was used for the negative stain. Multiple images with magnification from x10,000 to x40,000 were acquired.

Thioflavin T (ThT) fluorescence emission. The fluorescence emission of the 5 μM and 10 μM hIAPP were measured using a GloMax®-Multi Detection System (Promega; Wisconsin, USA). All samples were placed in a black 96 well-plate and mixed with 10 μM ThT aqueous solution. Fluorescence spectra of the samples were acquired every 45minutes with excitation at 405 nm and emission measurement at 490 nm, in a similar fashion to Chan *et al.*.[46-47]

Results and Discussion

Observation of the early oligomers formation in hIAPP. Aggregated hIAPP is composed of insoluble polypeptide fibrils, whose overall structure has been reported previously.[34, 48] The soluble oligomers are viable for MS study and can provide insights into the fundamental amino acid residue level binding between individual hIAPP monomer units and how they link together to form a higher order structure. Ultrahigh resolution MS allowed observation of the early oligomers of hIAPP via direct infusion without prior separation. Consecutive hIAPP oligomers, up to the pentamer, were detected in the nESI mass spectrum of the 10 μM hIAPP in aqueous solution with 2% DMSO residual present in the solvent (Figure 1B), suggesting hIAPP associates in a sequential process, with individual monomers attaching to growing oligomers. Despite very closely positioned oligomer peaks and overlapping isotopic envelopes with various charge states (5+ dimer/ 10+ tetramer and 2+ monomer/ 4+ dimer/ 6+ trimer), the isotopic patterns of each oligomer were still well-resolved. Observed signal intensity of the oligomers decreased with increasing size of oligomer species, suggesting observed species are early oligomers from sequential aggregation. Larger hIAPP oligomers above pentamer were not observed, which is attributed to oligomer's decreasing solubility and thus viability for nESI-MS. Similar observations of the oligomers' distribution pattern was found in the nESI mass spectrum of the 10 μM hIAPP in aqueous solution only (Figure S3).

The type of interaction between the early oligomers of hIAPP. The dimers and trimers of hIAPP (without conformer separation) were individually isolated and subjected to CAD MS/MS to determine the interactions between the hIAPP units. The 5+ charge state of hIAPP dimer was dissociated into 2+/3+ monomer peaks, and the 7+ charge state of hIAPP dimer was dissociated into 3+/4+ monomer peaks

(Figure 2A), indicating near-symmetrical charge distribution between monomer units. Excess CAD energy (at 14 V) during dimer dissociation resulted in the monomer fragmentation which yielded b and y ions, and reduced the monomer relative peak area. The dissociation of dimers into monomer hIAPP units in CAD MS/MS indicates the interactions between hIAPP units are fragile and non-covalent.

In the 8+ charge state trimer hIAPP (Figure 2B), the dissociation of trimer hIAPP resulted in the increase of hIAPP dimer from 15% to 29% between 0 V and 9 V; when the dissociation energy exceeded 10 V, the amount of dimer species decreased and resulted in a significant increase in the monomer hIAPP thereafter. The results demonstrated the oligomers of hIAPP are dissociating sequentially.

The aggregation site between the early oligomers of hIAPP. In order to gain sequence-specific hIAPP interaction information, the dimer and trimer ions of hIAPP (without conformer separation) were also studied via ECD MS/MS. The 5+ charge state dimer was isolated and fragmented using ECD (Figure S4) with summarised fragments shown in Figure 3B. Fragments observed included 1 monomer c-ion, 3 dimer c-ions, and 3 dimer z-ions (representing the mass of a hIAPP unit plus a c-/z-ion fragment). The M+c_{34} ion (representing mass equal to one hIAPP (M) plus a c_{34} ion from a second hIAPP unit) was the first c-ion dimer fragment observed from the 5+ hIAPP dimer spectrum, indicating the dimer interaction locates between Lys-1 and Ser-34. In addition, the M+z_{27} (representing mass equal to one hIAPP (M) plus a z_{27} ion from a second hIAPP unit) was the first z-ion dimer fragments observed from the 5+ hIAPP dimer ECD spectrum suggesting the dimer interaction also locates between Arg-11 and Tyr-37. IR-ECD was then used to enhance the fragmentation of the 5+

hIAPP dimer; 3 extra dimer z-ions, $M+z_{22}$ to $M+z_{24}$ were observed in the spectrum (Figure S5), which localises the dimer interaction region to between Leu-16 and Try-37.

Even though limited dimer fragments were obtained from the ECD MS/MS and the IR-ECD mass spectra of the 5+ dimer ion, the 7+ hIAPP dimer ion showed extensive fragmentation under ECD MS/MS (Figure 3A & S6) as the fragmentation efficiency in ECD MS/MS is directly proportional to the charge state of precursor ion.[49] With a higher charge state precursor ion, the ECD MS/MS of the 7+ hIAPP dimer ion produced 33 monomer c-ions, 4 monomer z-ions, 7 dimer c-ions, and 30 dimer z-ions (Figure 3C). The $M+c_{29}$ and $M+z_3$ ions were the first c-/z-ion observed from the 7+ hIAPP dimer, indicating the dimer interaction is located between Lys-1 and Ser-29 (proposed from the dimer c-ion fragments) as well as Asn-35 and Try-37 (proposed from the dimer z-ion fragment). Beyond the first association point of dimer hIAPP, sequential dimer fragment ions were also detected ($M+c_{31-36}$ and $M+z_{5-36}$).

The hIAPP trimer 8+ ion was also interrogated using ECD MS/MS. Compared to the previous hIAPP dimer spectrum, the ECD mass spectrum of the 8+ charge state trimer was more complex due to the presence of monomer, dimer, and trimer fragments simultaneously, though sequence informative fragments were successfully observed (Figure 3D & S7). Aside from the monomer and dimer fragments, trimer c- and z-ion (representing the mass of two hIAPP units plus a c-/z-ion fragment) were also obtained. 21 monomer c-ions, 2 dimer c-ions, 1 dimer z-ion, 3 trimer c-ions, and 24 trimer z-ions were identified from the ECD mass spectrum. The first

detectable trimer fragments were 2M+c34 and 2M+z5, indicating the third hIAPP unit associates with the dimer hIAPP between Lys-1 and Ser-34 (proposed from the trimer c-ion fragments) as well as Gly-33 and Try-37 (proposed from the trimer z-ion fragments). Beyond the first association point of trimer hIAPP, sequential trimer fragment ions were also detected ($2M+c_{35/36}$ and $2M+z_{6-36}$). Similar ECD MS/MS fragments were obtained from hIAPP dimer and trimer ions which were dissolved solely in aqueous solution (Figure S8), suggesting the presence of 2% DMSO in aqueous solutions does not affect the interactions between early oligomers of hIAPP.

The main limitation of the ECD MS/MS technique is to achieve the required cleavage coverage to reasonable localize the interaction region and how this may not always be achievable, especially with particularly low charge states for a given complex. Furthermore, all dimer and trimer fragments (M+c/z-ion and 2M+c/z-ion) in Figure 3 were used to determine the interaction regions between hIAPP units; the monomer fragments (c/z-ion) from the ECD mass spectra, however, were not considered for the structure elucidation of hIAPP aggregates due to the generation of hIAPP monomer during ECD fragmentation (Figure S4, S6, and S7). The observed monomer fragments (c/z-ion) were possible to be generated from either the oligomers or the monomer unit of hIAPP which might provide misleading results in determining the aggregation site of hIAPP; and the ECD MS/MS data obtained herein cannot differentiate the origins of the fragments. Thus, only dimer/trimer fragments (M+c/z-ion and 2M+c/z-ion) were applied in determining the interaction region between hIAPP aggregates.

The ECD spectrum of the 7+ charge state hIAPP dimer provided the highest

number of dimer fragments (M+c/z-ion) (Figure 3C) compared to other hIAPP oligomers' spectra. Previous literature has demonstrated application of ECD MS/MS fragmentation to determine the non-covalent interaction sites between protein-ligand via overlapping the proposed interaction regions observed from the first detectable c- and z-ions of proteins and linked ligands.[41, 51] This methodology, however, cannot apply to the 7+ charge state dimer as the interaction region proposed from the dimer c-ion is between Lys-1 and Ser-29, while the interaction region proposed from the dimer z-ion is between Asn-35 and Try-37,the proposed regions from dimer c- and z-ion are not overlapping (Figure 3B). In order to rationalise the fragments observed from the 7+ charge state dimer hIAPP, the only possible interaction between the dimer is asymmetric interaction between hIAPP units, indicating a residue-offset interaction occurs between hIAPPs (Figure 4A & 4B). From the fragments observed in the ECD mass spectra of 2% DMSO aqueous solution (Figure 3C) and pure aqueous solution (Figure S8B), we suggest the Ser-28 or Ser-29 residue of the first hIAPP unit are interacting with the Asn-35 residue on the second hIAPP unit (Figure 4A & 4B), thus the dimer fragments, $M+c_{28/29}$ and $M+z_3$ together with the sequential dimer fragment ions, were observed in the 7+ charge state dimer hIAPP ECD mass spectra (Figure 4D). This aggregation site also agrees with the fragments observed in the 5+ charge state hIAPP dimer ECD mass spectra. Due to a lower charge state in the 5+ hIAPP dimer, less fragments were observed compared to the 7+ hIAPP dimer. The first observable dimer fragments, $M+c_{34}$ and $M+z_{27}$, were possibly generated from the first hIAPP unit (Figure 4C) while the hIAPPs are still linking via the Ser-28/Ser-29 (the first hIAPP unit) and Asn-35 (the second hIAPP unit) residues.

The proposed aggregation site between hIAPP units not only agrees with the dimer interaction data presented, but more importantly it also applies to the trimer or even the higher orders hIAPP oligomers. With the asymmetric interaction between hIAPP units, the Ser-28/Ser-29 residue of the first hIAPP is interacting with the Asn-35 residue of the second hIAPP unit, in which the Ser-28/Ser-29 residue of the second hIAPP is still available for an interaction to the Asn-35 residue of the third hIAPP unit (Figure 4E). The first observable trimer fragments ($2M+c_{34}$ and $2M+z_5$) together with the sequential trimer fragments in the 8+ trimer hIAPP ECD MS/MS also support this aggregation site. The aggregation site proposed herein can further apply to the higher orders hIAPP oligomers to great lengths; at the same time, it agrees with Dupuis *et al.* research which suggests the interaction region between hIAPP units is located at β-sheet region.[33] The proposed aggregation site, Ser-28/29 and Asn-35, in hIAPP also agrees with the observation of Pramlintide in previous studies.[52-53] Pramlintide, a common injectable amylin for diabetes, has been shown not to aggregate in solution when the residues at Ala-25, Ser-28, and Ser-29 are replaced with Proline,[52-53] indicating their amyloidogenic influence.

Many studies of amyloid proteins have demonstrated the use of shorter peptide sections of possible amyloidogenic nature aggregate themselves.[4, 54] A synthetic 8-residue peptide (TNVGSNTY-NH_2) was then mixed with hIAPP in 1:1 molar ratio. The mixed-peptide mass spectrum showed hIAPP interacts with the synthetic peptide in various binding ratios (Figure 5A) as both hIAPP and synthetic peptides demonstrated an aggregation ability in isolation (Figure 1B and S9). The dissociation curve showed little CAD energy was required to disrupt the interaction between hIAPP species and the synthetic peptide, suggesting non-covalent interaction

is present between the molecules (Figure S10). The precursor ion of mixture composed of one hIAPP and one synthetic peptide was isolated and fragmented using ECD. The first observable hetero-dimer fragments on hIAPP were [TNVGSNTY+c_{32}] and [TNVGSNTY+z_{27}], indicating the interaction region of hIAPP with the synthetic peptide locates between Arg-11 and Val-32 (Figure 5B). However, the first observable hetero-dimer fragments on the synthetic peptide was [hIAPP+z_3] and no hetero-dimer c-ion fragments was observed (Figure 5B), indicating the interaction region of synthetic peptide locates between Asn-6 and Try-8 (position Asn-35 and Try-37 on the hIAPP). Ser-28/Ser-29 residue is not present on the synthetic peptide, thus the only binding motif of the synthetic peptide to hIAPP based on the interaction site proposed in Figure 4 is Asn-35 (Figure 5D); the hetero-dimer fragments of [hIAPP+z_3], therefore, agrees with the proposed aggregation site. However, Ser-28/Ser-29 will be the only possible binding motif on hIAPP for the synthetic peptide, the proposed interaction region (between Arg-11 and Val-32) based on the hetero-dimer fragments of hIAPP and synthetic peptide also agrees with this hypothesis (Figure 5C).

From soluble oligomers to mature and insoluble fibrils. hIAPP has been shown to oligomerise during incubation,[20, 55] where the soluble oligomers can combine and orientate into a β-sheet structure forming a mature, insoluble fibril. When hIAPP monomers aggregate, the concentration of free hIAPP monomer decreases, and as a result can be used to follow the extent and rate of hIAPP aggregation into oligomers.[56-57] In order to determine the aggregation rate, a 10 μM solution of hIAPP was incubated at 37ºC; the concentration of soluble hIAPP was then determined by comparison of relative MS peak area of the monomer in each

aliquot of the incubated sample over 28 days. A reduction in the percentage of soluble hIAPP was observed after the first week of incubation (Figure 6A). After 12 days incubation, ~ 50% reduction of the percentage of soluble hIAPP was observed. After 28 days incubation, only 25% of remaining soluble hIAPP monomer was observed in the 10 μM solution.

FTICR MS is well suited for the quantification of soluble proteins (such as hIAPP) in solution, but ESI is limited to soluble components only, and cannot effectively ionise the mature, insoluble fibrils. Thus, the relative concentration of amyloid fibril formed in the incubated solutions were determined using ThT fluorescence spectroscopy at emission 490 nm (Figure 6B), as used by Chan *et al.* previously.[46, 58] Both solutions showed limited detectable aggregation by ThT fluorescence for the first 40 hours of incubation (lag phase), followed by a sharp increase to a maximum value at around 55 hours. The end time relative fluorescence emission of the 10 μM hIAPP solution was 2.7 times higher than the fluorescence emission recorded in the 5 μM solution, indicating the aggregation rate of amyloid protein is directly proportional to the protein concentration TEM images of the (C) fresh, (D) 1-week, (E) 2-week, and (F) 4-week incubated 10 μM hIAPP solutions. The scale bars for each TEM image are inset.

The formation of amyloid fibrils in the 10 μM solutions was also monitored by TEM. Freshly solubilised hIAPP molecules clump together, which can be observed as small black clusters shown in the TEM images (Figure 6C). Loosely-packed and elongated fibrils were clearly observed in the TEM images of the 1-week incubated sample images (Figure 6D). The longest fibril observed within the 1-week incubated

solution was 5.1 μm. Long fibrils were still observed in the incubated 2-week sample (Figure 6E), along with shorter, more densely packed fibrils, showing a gradual change in the hIAPP fibril structure at longer incubation time. Very dense fibrils were observed at the 4-week stage (Figure 6F), showing little remaining space between the fibril branches shows the continuous decrease in the percentage of soluble hIAPP over one month, also observed in the incubated solutions measured using MS.

Conclusion

The experimental results here demonstrated the capabilities of MS in determining the aggregation region of amyloid protofibrils in gas phase down to the amino acid residue level as well as monitoring the long-term aggregation rate of amyloid protein, which are both challenging to observe using other current techniques. The most important aggregation regions between individual hIAPP units within oligomers in the gas phase occurs toward the C-terminus of the peptides, at Ser-28/Ser-29 of the first hIAPP unit and Asn-35 of the second hIAPP unit in an offset/staggered orientation. The aggregation sites of the dimer and trimer of hIAPP were shown by ECD MS/MS to be very similar, with both structures interacting primarily towards the C-terminus of the peptides, and the proposed aggregation site was further supported by the results obtained from the mixture of hIAPP and ^{30}TNVGSNTY^{37}-NH_2 peptide. Furthermore, this is the first-time the aggregation rate of hIAPP over a long period of time (one month) has been shown using MS relative quantification; it is difficult to observe or quantify the amyloid fibrillisation rate over a long period of time using fluorescence spectrometry and TEM respectively. The results of the long-term aggregation provides an opportunity to

monitor the long-term inhibition effects of the potential therapeutic in the future.

Supporting Information

The Supporting Information is available free of charge on the ACS Publications website.

CAD and ECD MS/MS spectra of hIAPP; MS spectrum of hIAPP in aqueous solution; ECD and IR-ECD MS/MS spectra with corresponding fragmentation map of hIAPP early oligomers (dimer and trimer); MS, dissociation curves, ECD fragmentation map, and TEM images of a segment of hIAPP; dissociation curve of hIAPP with a segment of hIAPP; assignment tables for CAD, ECD, and IR-ECD MS/MS experiments (PDF)

AUTHOR INFORMATION

Corresponding Author

*Peter O'Connor

p.oconnor@warwick.ac.uk

Notes

The authors declare no competing financial interest.

ACKNOWLEDGMENT

This research was supported by the funding from University of Warwick Research Development Fund (RD16003); Horizon 2020 EU FTICR MS network (project 731077); EPSRC (EP/F034210/1, EP/J000302/1, EP/N021630/1); BBSRC

(BB/R022399, BB/P021875); Funds for Women Graduates; and Great Britain China Centre. The authors would also like to thank Dr. Maria A. van Agthoven, Dr. Andrea Lopez-Clavijo, and Ms Meng Li for their helpful comments and suggestions.

REFERENCES

1. Koo, E. H.; Lansbury, P. T.; Kelly, J. W., Amyloid diseases: abnormal protein aggregation in neurodegeneration. *Proc. Natl. Acad. Sci. USA* **1999,** *96* (18), 9989-9990.
2. Conway, K. A.; Lee, S. J.; Rochet, J. C.; Ding, T. T.; Williamson, R. E.; Lansbury, P. T., Acceleration of oligomerization, not fibrillization, is a shared property of both alpha-synuclein mutations linked to early-onset Parkinson's disease: Implications for pathogenesis and therapy. *Proc. Natl. Acad. Sci. USA* **2000,** *97* (2), 571-576.
3. Cao, P.; Abedini, A.; Wang, H.; Tu, L.-H.; Zhang, X.; Schmidt, A. M.; Raleigh, D. P., Islet amyloid polypeptide toxicity and membrane interactions. *Proc. Natl. Acad. Sci. USA* **2013,** *110* (48), 19279-19284.
4. Bleiholder, C.; Dupuis, N. F.; Wyttenbach, T.; Bowers, M. T., Ion mobility-mass spectrometry reveals a conformational conversion from random assembly to beta-sheet in amyloid fibril formation. *Nat. Chem.* **2011,** *3* (2), 172-177.
5. Makin, O. S.; Atkins, E.; Sikorski, P.; Johansson, J.; Serpell, L. C., Molecular basis for amyloid fibril formation and stability. *Proc. Natl. Acad. Sci. USA* **2005,** *102* (2), 315-320.
6. Paul, W. E.; Cohen, A. S., Electron Microscopic studies of Amyloid Fibrils with Ferritinconjugated Antibody. *Am. J. Pathol.* **1963,** *43*, 721-38.
7. Shirahama, T.; Cohen, A. S., High-resolution electron microscopic analysis of the amyloid fibril. *J. Cell Biol.* **1967,** *33* (3), 679-708.
8. Volpatti, L. R.; Vendruscolo, M.; Dobson, C. M.; Knowles, T. P., A clear view of polymorphism, twist, and chirality in amyloid fibril formation. *ACS nano* **2013,** *7* (12), 10443-10448.
9. Cooper, G. J. S.; Day, A. J.; Willis, A. C.; Roberts, A. N.; Reid, K. B. M.; Leighton, B., Amylin and the amylin gene: structure, function and relationship to islet amyloid and to diabetes mellitus. *Biochim. Biophys. Acta* **1989,** *1014* (3), 247-258.
10. Kahn, S. E.; Dalessio, D. A.; Schwartz, M. W.; Fujimoto, W. Y.; Ensinck, J. W.; Taborsky, G. J.; Porte, D., Evidence of cosecretion of islet amyloid polypeptide and insulin by beta-cells. *Diabetes* **1990,** *39* (5), 634-638.
11. Jaikaran, E.; Clark, A., Islet amyloid and type 2 diabetes: from molecular

misfolding to islet pathophysiology. *Biochim. Biophys. Acta-Mol. Basis Dis.* **2001,** *1537* (3), 179-203.
12. Luca, S.; Yau, W. M.; Leapman, R.; Tycko, R., Peptide conformation and supramolecular organization in amylin fibrils: Constraints from solid-state NMR. *J. Biochem.* **2007,** *46* (47), 13505-13522.
13. Williamson, J. A.; Miranker, A. D., Direct detection of transient alpha-helical states in islet amyloid polypeptide. *Protein Sci.* **2007,** *16* (1), 110-117.
14. Westermark, G. T.; Westermark, P.; Berne, C.; Korsgren, O.; Nordic Network Clin Islet, T., Widespread amyloid deposition in transplanted human pancreatic islets. *N. Engl. J. Med.* **2008,** *359* (9), 977-979.
15. Ashcroft, F. M.; Rorsman, P., Diabetes mellitus and the β cell: the last ten years. *Cell* **2012,** *148* (6), 1160-1171.
16. Westermark, P.; Engstrom, U.; Johnson, K. H.; Westermark, G. T.; Betsholtz, C., Islet Amyloid Polypeptide - Pinpointing Amino-Acid residues Linked to Amyloid Fibril Formation. *Proc. Natl. Acad. Sci. USA* **1990,** *87* (13), 5036-5040.
17. Wiltzius, J. J. W.; Sievers, S. A.; Sawaya, M. R.; Eisenberg, D., Atomic structures of IAPP (amylin) fusions suggest a mechanism for fibrillation and the role of insulin in the process. *Protein Sci.* **2009,** *18* (7), 1521-1530.
18. Fernandez, M. S., Human IAPP amyloidogenic properties and pancreatic beta-cell death. *Cell Calcium* **2014,** *56* (5), 416-427.
19. Laghaei, R.; Mousseau, N.; Wei, G., Effect of the Disulfide Bond on the Monomeric Structure of Human Amylin Studied by Combined Hamiltonian and Temperature Replica Exchange Molecular Dynamics Simulations. *J. Phys. Chem. B* **2010,** *114* (20), 7071-7077.
20. Akter, R.; Cao, P.; Noor, H.; Ridgway, Z.; Tu, L. H.; Wang, H.; Wong, A. G.; Zhang, X. X.; Abedini, A.; Schmidt, A. M.; Raleigh, D. P., Islet Amyloid Polypeptide: Structure, Function, and Pathophysiology. *J. Diabetes Res.* **2016**, 18.
21. Mishra, R.; Geyer, M.; Winter, R., NMR Spectroscopic Investigation of Early Events in IAPP Amyloid Fibril Formation. *ChemBioChem* **2009,** *10* (11), 1769-1772.
22. Ashburn, T. T.; Lansbury, P. T., Interspecies Sequences Variations Affect the Kinetics and Thermodynamics of Amyloid Formation: Peptide Models of Pancreatic Amyloid. *J. Am. Chem. Soc.* **1993,** *115* (23), 11012-11013.
23. Azriel, R.; Gazit, E., Analysis of the structural and functional elements of the minimal active fragment of islet amyloid polypeptide (IAPP) - An experimental support for the key role of the phenylalanine residue in amyloid formation. *J. Biol. Chem.* **2001,** *276* (36), 34156-34161.
24. Rhoades, E.; Agarwal, J.; Gafni, A., Aggregation of an amyloidogenic fragment of human islet amyloid polypeptide. *Biochim. Biophys. Acta-Protein Struct. Molec.*

Enzym. **2000,** *1476* (2), 230-238.
25. Tenidis, K.; Waldner, M.; Bernhagen, J.; Fischle, W.; Bergmann, M.; Weber, M.; Merkle, M. L.; Voelter, W.; Brunner, H.; Kapurniotu, A., Identification of a penta- and hexapeptide of islet amyloid polypeptide (IAPP) with amyloidogenic and cytotoxic properties. *J. Mol. Biol.* **2000,** *295* (4), 1055-1071.
26. Zanuy, D.; Porat, Y.; Gazit, E.; Nussinov, R., Peptide sequence and amyloid formation: Molecular simulations and experimental study of a human islet amyloid polypeptide fragment and its analogs. *Structure* **2004,** *12* (3), 439-455.
27. Scrocchi, L. A.; Chen, Y.; Waschuk, S.; Wang, F.; Cheung, S.; Darabie, A. A.; McLaurin, J.; Fraser, P. E., Design of peptide-based inhibitors of human islet amyloid polypeptide fibrillogenesis. *J. Mol. Biol.* **2002,** *318* (3), 697-706.
28. Rhoades, E.; Gafni, A., Micelle formation by a fragment of human islet amyloid polypeptide. *Biophys. J.* **2003,** *84* (5), 3480-3487.
29. Buchanan, L. E.; Dunkelberger, E. B.; Tran, H. Q.; Cheng, P.-N.; Chiu, C.-C.; Cao, P.; Raleigh, D. P.; de Pablo, J. J.; Nowick, J. S.; Zanni, M. T., Mechanism of IAPP amyloid fibril formation involves an intermediate with a transient β-sheet. *Proc. Natl. Acad. Sci. USA* **2013,** *110* (48), 19285-19290.
30. Sawaya, M. R.; Sambashivan, S.; Nelson, R.; Ivanova, M. I.; Sievers, S. A.; Apostol, M. I.; Thompson, M. J.; Balbirnie, M.; Wiltzius, J. J. W.; McFarlane, H. T.; Madsen, A. Ø.; Riekel, C.; Eisenberg, D., Atomic structures of amyloid cross-β spines reveal varied steric zippers. *Nature* **2007,** *447* (7143), 453-457.
31. Young, L. M.; Saunders, J. C.; Mahood, R. A.; Revill, C. H.; Foster, R. J.; Tu, L.-H.; Raleigh, D. P.; Radford, S. E.; Ashcroft, A. E., Screening and classifying small-molecule inhibitors of amyloid formation using ion mobility spectrometry-mass spectrometry. *Nat. Chem.* **2015,** *7* (1), 73-81.
32. Young, L. M.; Cao, P.; Raleigh, D. P.; Ashcroft, A. E.; Radford, S. E., Ion Mobility Spectrometry-Mass Spectrometry Defines the Oligomeric Intermediates in Amylin Amyloid Formation and the Mode of Action of Inhibitors. *J. Am. Chem. Soc.* **2014,** *136* (2), 660-670.
33. Dupuis, N. F.; Wu, C.; Shea, J. E.; Bowers, M. T., The Amyloid Formation Mechanism in Human IAPP: Dimers Have beta-Strand Monomer-Monomer Interfaces. *J. Am. Chem. Soc.* **2011,** *133* (19), 7240-7243.
34. Dupuis, N. F.; Wu, C.; Shea, J. E.; Bowers, M. T., Human Islet Amyloid Polypeptide Monomers Form Ordered beta-hairpins: A Possible Direct Amyloidogenic Precursor. *J. Am. Chem. Soc.* **2009,** *131* (51), 18283-18292.
35. Young, L. M.; Tu, L.-H.; Raleigh, D. P.; Ashcroft, A. E.; Radford, S. E., Understanding co-polymerization in amyloid formation by direct observation of mixed oligomers. *Chem. Sci.* **2017,** *8* (7), 5030-5040.

36. Kanu, A. B.; Dwivedi, P.; Tam, M.; Matz, L.; Hill, H. H., Jr., Ion mobility-mass spectrometry. *J. Mass Spectrom.* **2008,** *43* (1), 1-22.
37. Uetrecht, C.; Rose, R. J.; van Duijn, E.; Lorenzen, K.; Heck, A. J. R., Ion mobility mass spectrometry of proteins and protein assemblies. *Chem. Soc. Rev.* **2010,** *39* (5), 1633-1655.
38. Haataja, L.; Gurlo, T.; Huang, C. J.; Butler, P. C., Islet amyloid in type 2 diabetes, and the toxic oligomer hypothesis. *Endocr. Rev.* **2008,** *29* (3), 303-316.
39. Breuker, K.; McLafferty, F. W., Native electron capture dissociation for the structural characterization of noncovalent interactions in native cytochrome c. *Angew. Chem. Int. Ed.* **2003,** *42* (40), 4900-4904.
40. Robinson, C. V.; Chung, E. W.; Kragelund, B. B.; Knudsen, J.; Aplin, R. T.; Poulsen, F. M.; Dobson, C. M., Probing the nature of noncovalent interactions by mass spectrometry. A study of protein− CoA ligand binding and assembly. *J. Am. Chem. Soc.* **1996,** *118* (36), 8646-8653.
41. Xie, Y.; Zhang, J.; Yin, S.; Loo, J. A., Top-down ESI-ECD-FT-ICR mass spectrometry localizes noncovalent protein-ligand binding sites. *J. Am. Chem. Soc.* **2006,** *128* (45), 14432-14433.
42. Abedini, A.; Singh, G.; Raleigh, D. P., Recovery and purification of highly aggregation-prone disulfide-containing peptides: Application to islet amyloid polypeptide. *Anal. Biochem.* **2006,** *351* (2), 181-186.
43. Caravatti, P.; Allemann, M., The 'Infinity Cell': a New Trapped-ion Cell With Radiofrequency Covered Trapping Electrodes for Fourier Transform Ion Cyclotron Resonance Mass Spectrometry. *Org. Mass Spectrom.* **1991,** *26* (5), 514-518.
44. de Koning, L. J.; Nibbering, N. M. M.; van Orden, S. L.; Laukien, F. H., Mass selection of ions in a Fourier transform ion cyclotron resonance trap using correlated harmonic excitation fields (CHEF). *Int. J. Mass spectrom.* **1997,** *165*, 209-219.
45. Horn, D. M.; Ge, Y.; McLafferty, F. W., Activated ion electron capture dissociation for mass spectral sequencing of larger (42 kDa) proteins. *Anal. Chem.* **2000,** *72* (20), 4778-4784.
46. Chan, F. T. S.; Schierle, G. S. K.; Kumita, J. R.; Bertoncini, C. W.; Dobson, C. M.; Kaminski, C. F., Protein amyloids develop an intrinsic fluorescence signature during aggregation. *Analyst* **2013,** *138* (7), 2156-2162.
47. Yang, T.; Wang, X. H.; Zhang, C. L.; Ma, X.; Wang, K.; Wang, Y. Q.; Luo, J.; Yang, L.; Yao, C.; Wang, X. Y., Specific self-monitoring of metal-associated amyloid-beta peptide disaggregation by a fluorescent chelator. *Chem. Commun.* **2016,** *52* (11), 2245-2248.

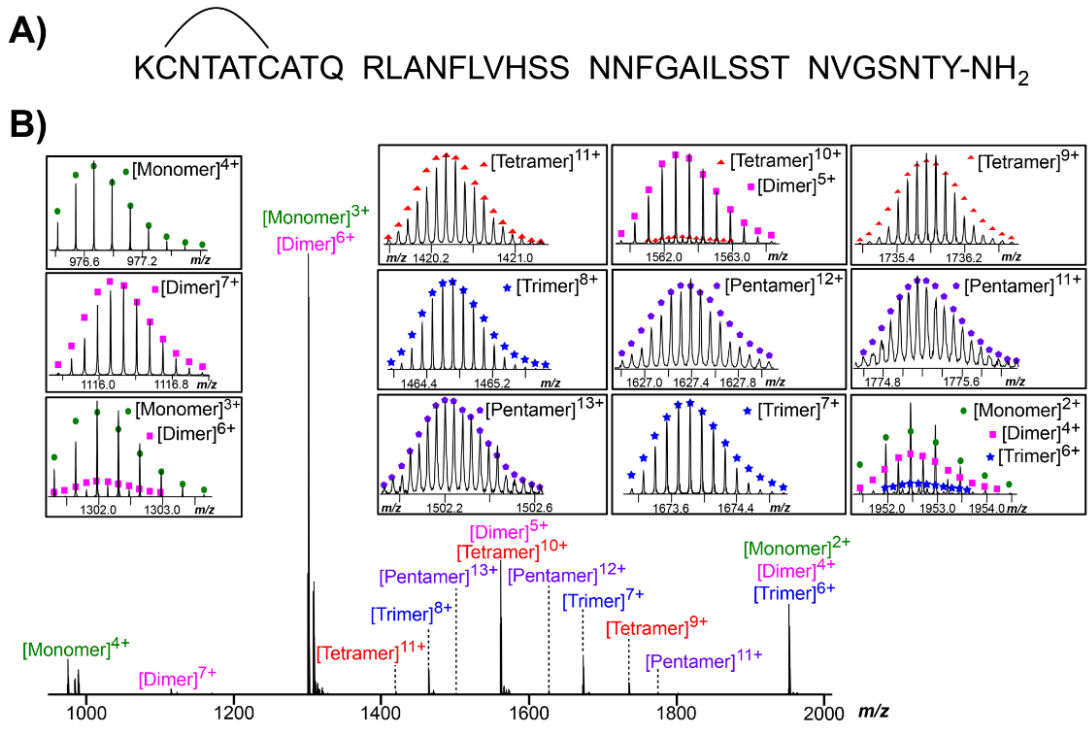

Figure 1. (A) The amino acid sequence of hIAPP. An intramolecular disulfide bond is located between Cys-2 and Cys-7, and hIAPP has an ami-dated C-terminus. (B) An nESI mass spectrum of the early oligomers from the 10 μM hIAPP aqueous solution with 2% (v/v) residual DMSO. Col-oured shapes represent the calculated isotope distributions for the different species overlaid onto the observed pattern.

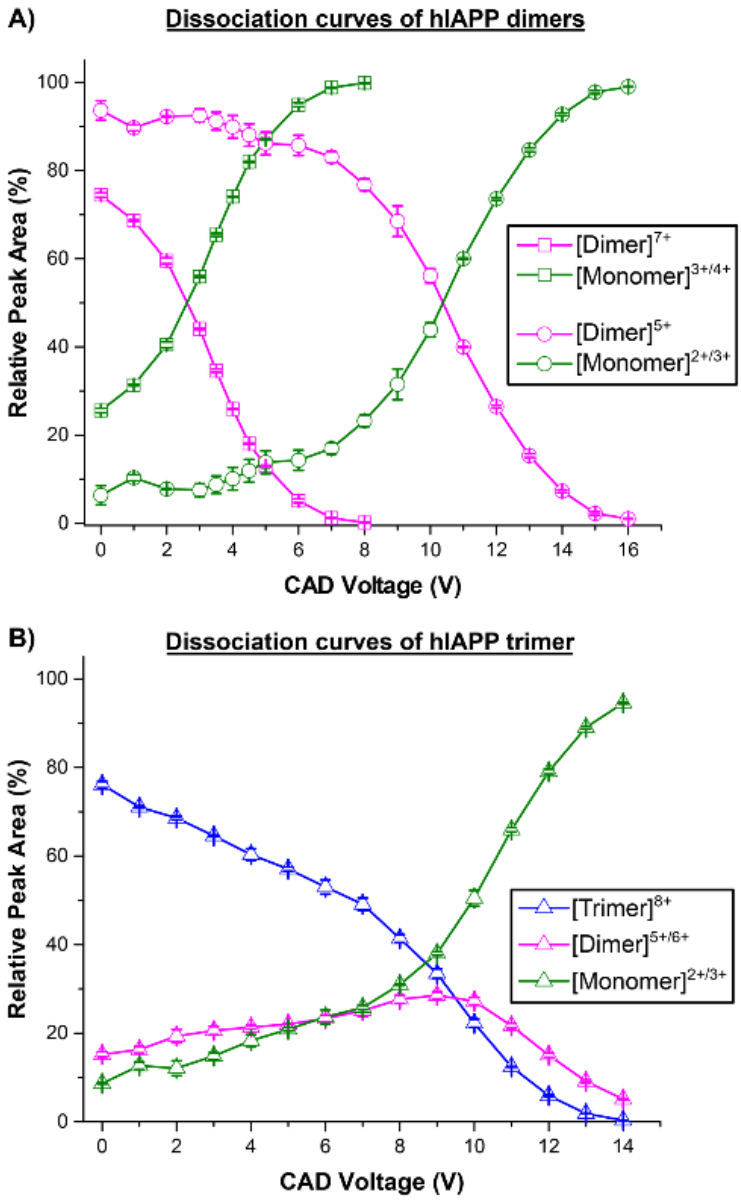

Figure 2. The relative peak areas of the monomer, the dimer, and the trimer ions during the dissociation of (A) the 5+ and 7+ charge state of hIAPP dimers as well as (B) the 8+ charge state of hIAPP trimer.

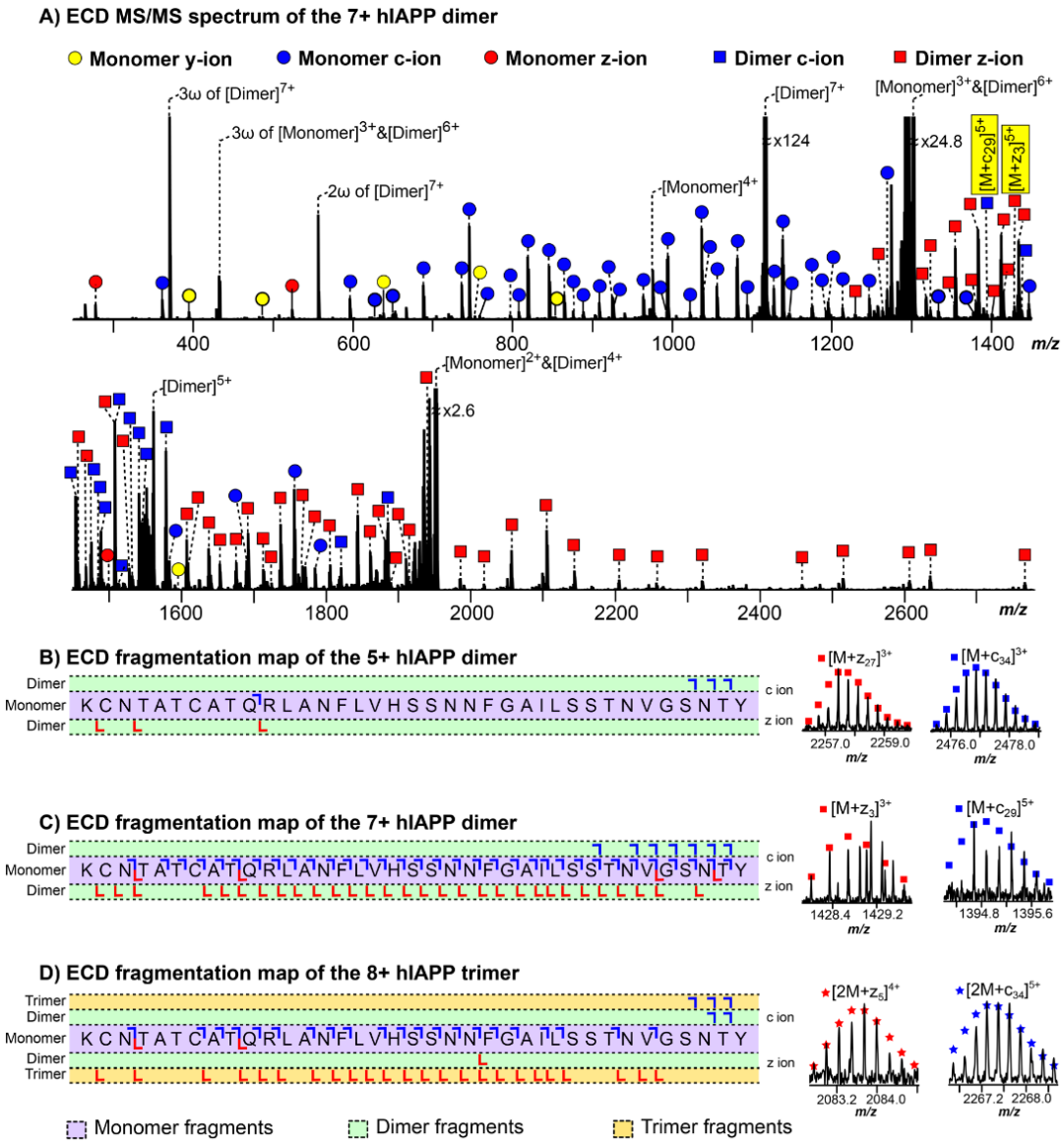

Figure 3. (A) ECD mass spectrum of the 7+ charge state hIAPP dimer. Yellow boxes fragments represent the critical dimer c- and z-ion observed. Summarised fragments observed in the ECD mass spectrum of the (B) 5+ dimer, (C) 7+ dimer, and (D) 8+ trimer of hIAPP. Examples of the critical assigned dimer/ trimer c- and z-ions from the ECD MS/MS are inserted. Coloured shapes represent the calculated isotope distributions.

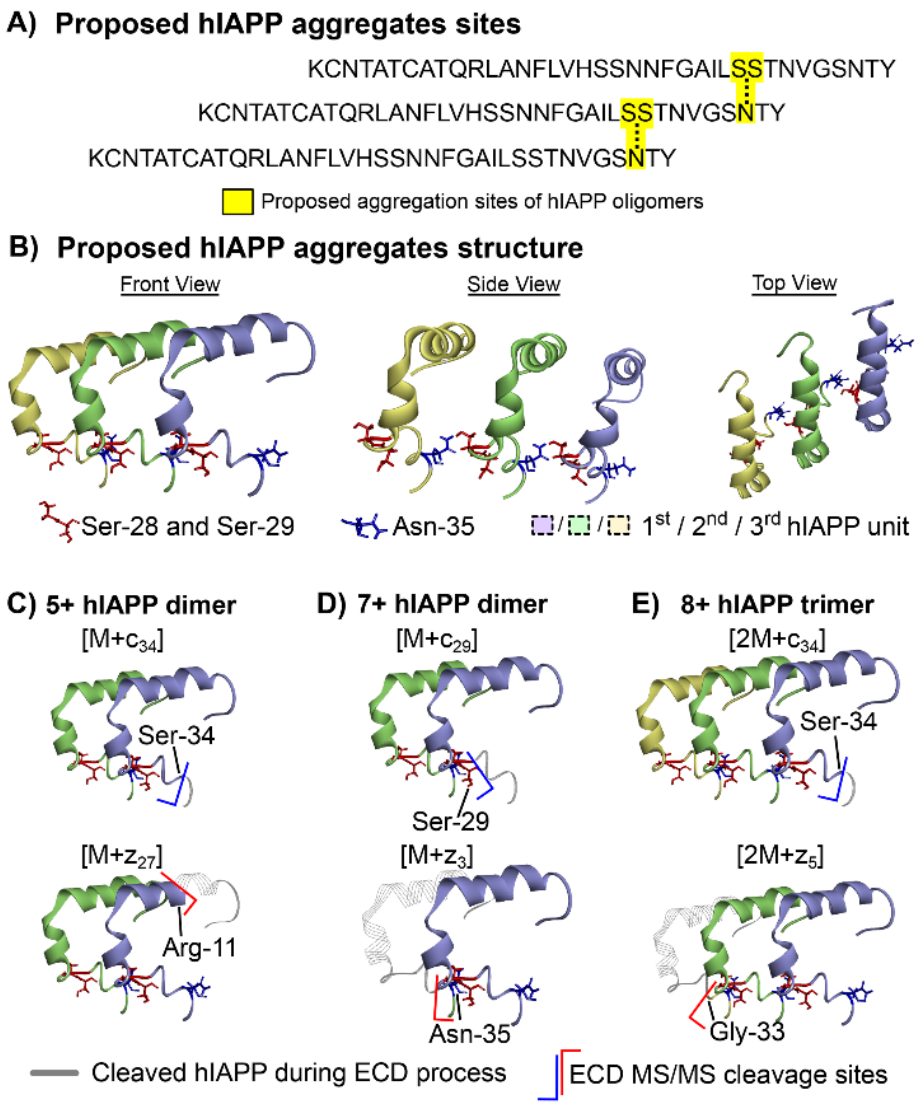

Figure 4. Proposed hIAPP aggregates (A) sites and (B) structure (PDB 2L86)[50] based on the ECD MS/MS fragments observed in Figure 3. Proposed hIAPP fragment structures for the (C) 5+ hIAPP dimer, (D) 7+ hIAPP dimer, and (E) 8+ hIAPP trimer. Grey regions of protein show cleaved portions during ECD MS/MS.

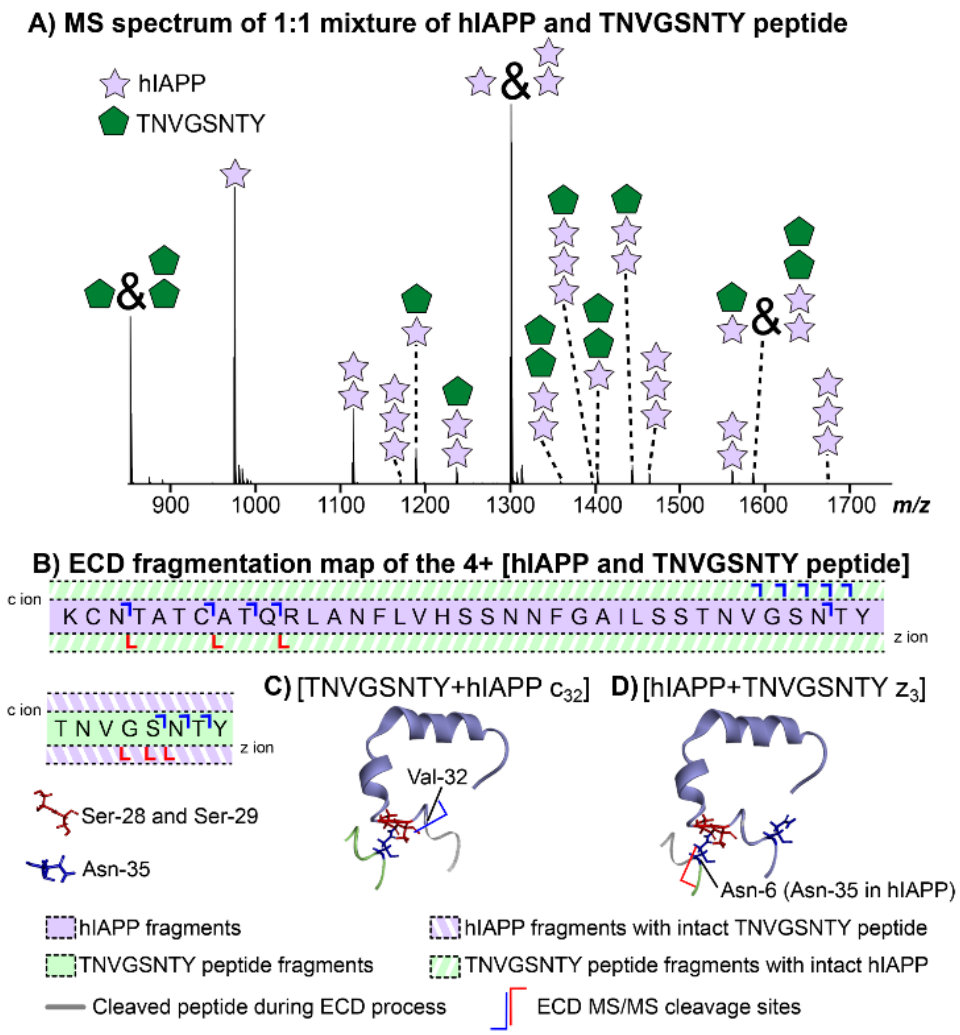

Figure 5. (A) Mass spectrum of the 1:1 mixture of hIAPP and the synthetic peptide (TNVGSNTY-NH2). (B) The summarised frag-mentation map of the 4+ charge state mixture of hIAPP and the synthetic peptide. The proposed molecular structure of the hetero-dimer (C) c and (D) z fragments.

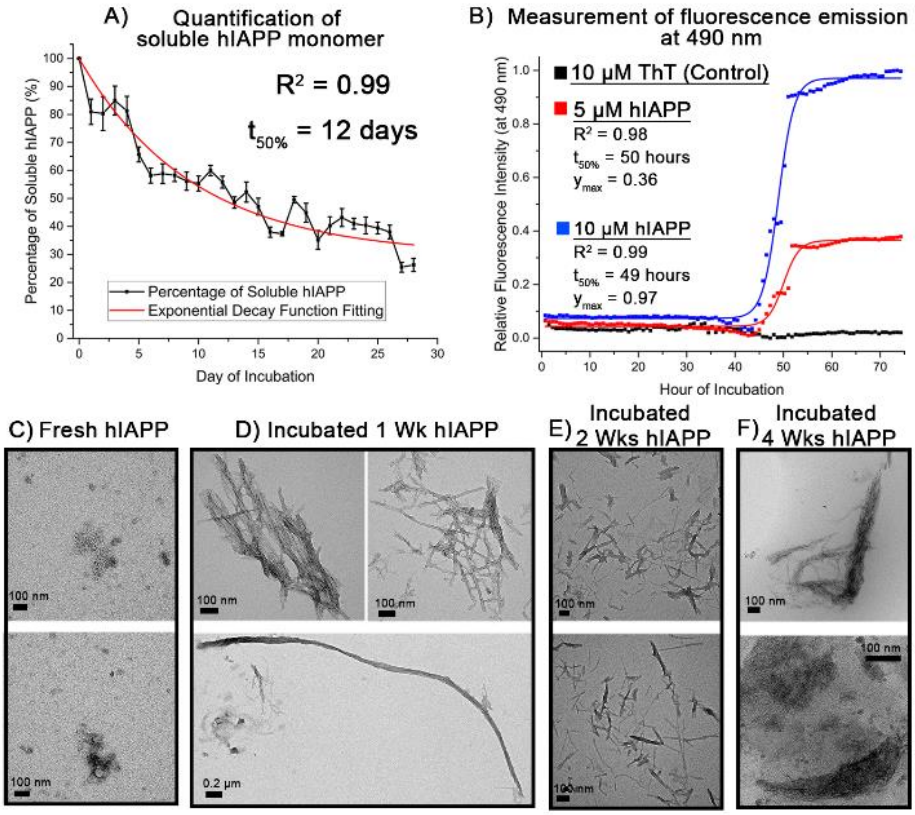

Figure 6. (A) Plot showing the amount of soluble hIAPP in the 10 μM solution changing over time measured using MS. (B) The relative fluorescence emission intensity of the 10 μM ThT solution, incubated 5 μM and 10 μM hIAPP solutions measured at emission 490 nm. The TEM images of the (C) fresh, (D) 1-week, (E) 2-week, and (F) 4-week incubated 10 μM hIAPP solutions. The scale bars for each TEM image are inset.